Final Draft

of the original manuscript

Lee, H.J.; Yi, S.; Letzig, D.; Park, N.:

Microstructure and Texture Evolution During the Heat Treatment of 0.6Zn–0.6Ca–Mg Alloy Sheet Manufactured via Twin Roll Casting

In: Metals and Materials International. Vol. 29 (2023) 2955-2964.

First published online by Springer: 01.04.2023

https://dx.doi.org/10.1007/s12540-023-01430-w

Microstructure and texture evolution during the heat treatment of 0.6Zn-0.6Ca-Mg alloy sheet manufactured via twin roll casting

Hee Jae Lee[1], Sangbong Yi[2,3]*, Dietmar Letzig[2], No-Jin Park[1]*

[1]School of Advanced Materials Science and Engineering, Kumoh National Institute of Technology, 61 Daehak-ro, Gumi, Gyeongbuk 39177, Republic of Korea

[2]Institute of Material and Process Design, Helmholtz-Zentrum Hereon, Max-Planck-Strasse 1, 21502 Geesthacht, Germany

[3]Department of Magnesium, Korea Institute of Materials Science, Changwon 51508, Republic of Korea

***Corresponding authors**:

No-Jin Park

School of Advanced Materials Science and Engineering, Kumoh National Institute of Technology

61 Daehak-ro, Gumi, Gyeongbuk 39177, Republic of Korea

E-mail: njpark@kumoh.ac.kr

Sangbong Yi

Institute of Material and Process Design, Helmholtz-Zentrum Hereon

Max-Planck-Strasse 1, 21502 Geesthacht, Germany

Email: sangbong.yi@hereon.de

Acknowledgements

This research was supported by Kumoh National Institute of Technology (2021). Financial support of BrainPool Program (Grant nr. 2021H1D3A2A0208305) of National Research Foundation and KIMS Academy Lab program (PNK8660) for the research stay of SYi at KIMS is gratefully acknowledged.

Abstract

This study examined the microstructure evolution during the thermomechanical treatments of the twin roll cast strip of magnesium alloy. Magnesium alloy composed of 0.6wt% Zn and 0.6wt% Ca was manufactured by TRC and subsequently rolled at 370°C, and the rolled sheets were heat treated at 400°C for various periods of time. In the as-TRC plate, the dendritic cast structure inclined in the rolling direction was observed with the centerline segregation. The as-rolled sheet shows a mixture of fine recrystallized grains and the remaining cast structure. The annealing at 400°C brings about the recrystallization and a gradual grain coarsening for 16 h. After the 16 h heat treatment, secondary recrystallization accompanying the abnormal grain growth was observed, which is attributed to the easier grain boundary motion resulting from the dissolution of Mg_2Ca and $Ca_2Mg_5Zn_5$ precipitates. The as-TRC plate shows a basal-type texture with a slight basal pole spread in the transverse direction, whereas the basal poles tilted by approximately 10˚ in the rolling direction are formed in the rolled sheet. During the 2 h heat treatment, the texture significantly weakens accompanying the formation of the basal poles inclined by approximately 30° in the transverse direction. These results suggest that a homogeneous microstructure with a weak texture can be obtained by the hot-rolling and heat treatments of the TRC plate, which is advantageous for an improved sheet formability, whereas the heat treatment longer than 16 h causes abnormal grain growth.

Keywords: Mg alloy; Twin Roll Casting; Homogenization; Texture; Heat-treatment

1. Introduction

Magnesium and its alloys can contribute to the weight reduction of portable electronic devices and transportation vehicles owing to the lowest density among the commercially available metallic materials and their high specific strength [1]. Their potential for application in lightweight structures has attracted the researchers over decades to draw a property-microstructure relationship to achieve a wide range of diverse industrial applications, especially in the transportation sectors [2, 3]. Plastic deformation of the magnesium alloys are accommodated by the dislocation slip activated on the basal and / or non-basal (prismatic and pyramidal) planes. Plastic deformation, especially at room temperature, occurs mainly by activation of the basal dislocation slip and mechanical twinning, while the activation of non-basal dislocations are highly restricted owing to their high critically resolved shear stresses (CRSS) compared to that for the basal dislocation. With the increasing temperature, the CRSS of the non-basal dislocations slip rapidly decreases and the magnesium alloys become more ductile, such that the mechanical processing of the commercial magnesium alloys, such as AZ31, is conducted at an elevated temperature, usually at a temperature higher than 180 °C, which increases the manufacturing costs [4]. Wrought processes, such as rolling and extrusion, of the commercial magnesium alloys result in the formation of a strong basal-type texture [5], which results in a strong mechanical anisotropy and poor formability at room temperature. Many studies have been conducted to modify the microstructure and texture by optimization of the process and / or alloy composition, and texture control has been acknowledged as an effective way to overcome the poor formability. [1, 6-12].

Twin roll casting (TRC) process combines the solidification and rolling deformation in a process step, in which the molten metal is injected directly into the roll gap to produce a plate of the desired thickness [13]. Because a relatively thin TRC plate can be directly processed without further machining or long homogenization treatment, the production cycles to the final sheet thickness can be dramatically reduced using the TRC process [14, 15]. In addition to the economic benefits based on the increased productivity, the sheet properties are also improved by sheet processing via TRC due to a rapid cooling rate and consequent microstructural changes. The TRC strips usually exhibit an inhomogeneous microstructure, such as central segregation and inverse segregation [7, 8, 16]. A previous study indicated the formation of a strong texture with an inhomogeneous microstructure of a TRC plate of Mg-Zn-Ca alloy, while the microstructural inhomogeneity and texture diminish by heat treatments [9].

The ultimate goal of this study is to provide a guideline towards the improved formability of Mg-Zn-Ca alloy strips manufactured through the TRC process by controlling the inhomogeneous microstructure and strong texture through subsequent thermomechanical treatments, such as hot rolling and recrystallization annealing.

2. Experimental

In this study, a magnesium alloy composed of 0.6 wt.% Zn and 0.6 wt.% Ca was molten at 715°C. Furthermore, a strip with a thickness of 5 mm was manufactured through TRC process. The rolling speed during the TRC was 2.5 m/min. The TRC strip was hot rolled in five passes at 370°C. The first pass reduced the thickness to 4 mm. The subsequent 2nd to 5th passes reduced the thickness by 0.5 mm with each pass, and a final thickness of 2 mm was obtained, as shown in Fig. 1. To analyze the change in the microstructure during the heat treatment, the rolled sheet was heat treated at 400°C for 2, 4, 8, 16, 32, and 64 h and then air-cooled. The change in the microstructure was analyzed at the sheet normal plane (RD-TD plane) and the sheet transverse plane (RD-ND plane) using an optical microscope (BX41M-LED). The specimens for the optical microscopy were mechanically ground to #4000 emery paper, and then polished using 0.3 μm diamond paste. The polished samples were etched using a picric acid-based etchant (100 ml D.I. water, 100 ml ethanol, 6 ml acetic acid, 2 g picric acid). The average grain sizes were determined by linear intercept method using a micrograph covering more than 2000 grains, that corresponds to the area coverage of approximately 1500 x 2000 μm^2. To analyze the elements distribution and the chemical compositions of precipitates and segregation sites, EDS analysis was performed in a FEG-SEM (MAIA 3, TESCAN).

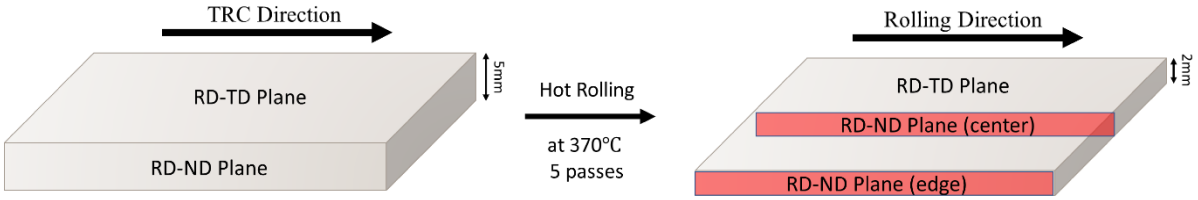

Fig. 1 Schematics of the examined samples

The planes of the observation for optical microscopy are marked with red rectangles

The macro-texture of each sample was measured at the RD-TD plane using an X-ray diffractometer (D-5005, Bruker AXS) by tilting the specimen by 70° with the step size of 5°. The orientation distribution function (ODF) was calculated using six measured pole figures, $\{10\bar{1}0\}$, (0002), $\{10\bar{1}1\}$, $\{10\bar{1}2\}$, $\{11\bar{2}0\}$, $\{10\bar{1}3\}$, by applying the triclinic specimen coordinate system [17]. Specimens for electron backscatter diffraction (EBSD)

analysis were prepared by electropolishing in a Struers AC2 solution at -20°C and 30 V. The EBSD measurements were conducted using a field emission gun scanning electron microscope (working at 15 kV, Zeiss Crossbeam 550L, Carl Zeiss AG, Oberkochen, Germany) equipped with a Symmetry detector (Oxford Inc.) and an AZTEC EBSD system on a measuring area of 1900 × 1500 μm^2 with a step size of 1 μm at the RD-TD plane.

3. Results and Discussion

The optical microstructure of the TRC strip is shown in Fig. 2. A columnar structure with the fine dendrites is observed in the RD-ND plane. The columnar structure close to the strip surface is inclined to the RD, while a globular cast structure is developed at the mid-thickness area, as shown in Fig. 2(a). At the mid-thickness area, a heavy segregation zone marked with a dashed circle, is observed, as shown in Fig. 2(b). Central segregation is caused by the solidification from the surface towards the mid-thickness zone; for example, the growth of the columnar grains. Such directional solidification results in a higher concentration of alloying elements at the mid-thickness zone and, consequently, the formation of the centerline segregation along the RD of the TRC strip. [7, 18]. Such microstructural inhomogeneity is usually developed in the TRC strips. In our previous study [9], it was found that a relatively homogeneous microstructure with the average grain size of 20 μm could be achieved through recrystallization annealing of the TRC plate at 400°C for 2 h. Notably, the rolling deformation applied to the strip during TRC allows the possible microstructure tailoring by recrystallization annealing in addition to the homogenization.

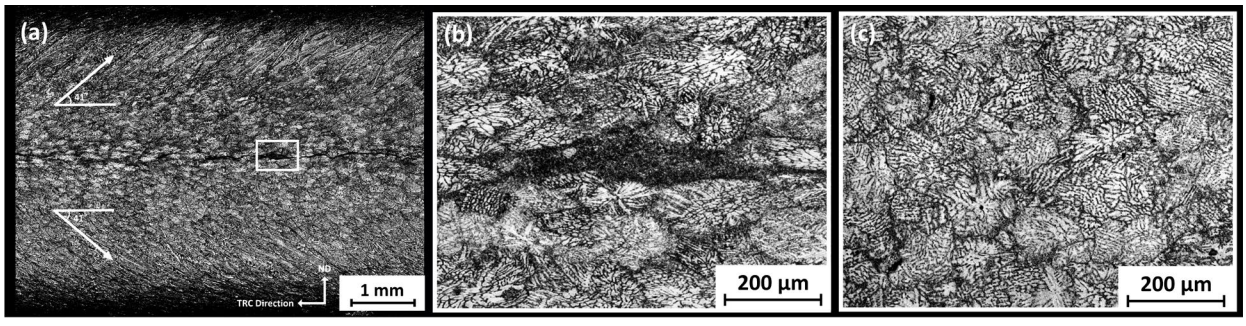

Fig. 2 Optical micrographs of the as-TRC plate with the thickness of 5 mm at (a) RD-ND plane, (b) magnified view of the centerline segregation at the mid-thickness layer, and (c) RD-TD plane

Fig. 3 demonstrates the optical microstructure of the sheet rolled to a thickness of 2 mm. The rolled sheet has a mixture of fine recrystallized grains, with the average grain size of 6 μm, and the dendritic cast structure. The cast structure in the rolled sheet was further tilted in the RD (Fig. 3(a)) compared to those in the

TRC strip, and the central segregation is observed after the hot rolling. Cracks formed at an angle of approximately 45° to the RD at the edge of the rolled sheet, as shown in Fig. 3(b), while there was no cracking in the central part of the rolled sheet. Additionally, the cast structure at the edge of the rolled sheet is irregularly inclined and arranged, as the cracks occur. The microstructure evolution during the heat treatment at 400°C for 2, 4, 8, 16, 32, and 64 h are shown in Fig. 4. From Fig. 4(a), it can be observed that the recrystallization was completed after 2 h heat treatment and the dendritic cast structure and non-uniform microstructure observed in the as-rolled sheet, including the mid-thickness segregation, almost disappeared. Grain growth occurred with the increasing heat treatment time, and secondary recrystallization occurred, in which only some grains showed an abnormal growth. The grain growth behavior during the heat treatment was estimated in terms of the average grain size and the fraction of abnormally grown grains, as shown in Fig. 5. The average grain size of the heat-treated sample for 2 h was 8.0 μm, and the grain size evolved to 8.2 μm, 8.7 μm, 10.1 μm, 11.9 μm, and 50.0 μm after 4 h, 8 h, 16 h, 32 h, and 64 h, respectively. A gradual grain growth was observed in the 32 h heat treated sample, whereas the 64 h heat treated sample showed a sharp increase in the average grain size. Notably, some largely growing grains are found in the 8 h heat treated sample and the fraction of such abnormally growing grains suddenly increased after 32 h heat treatment. In the 64-h heat treated sample, the area fraction of the abnormally growing grain reached to 75.1%, and the grains much larger than 500 μm were mixed with relatively fine grains, as shown in Fig. 4(f).

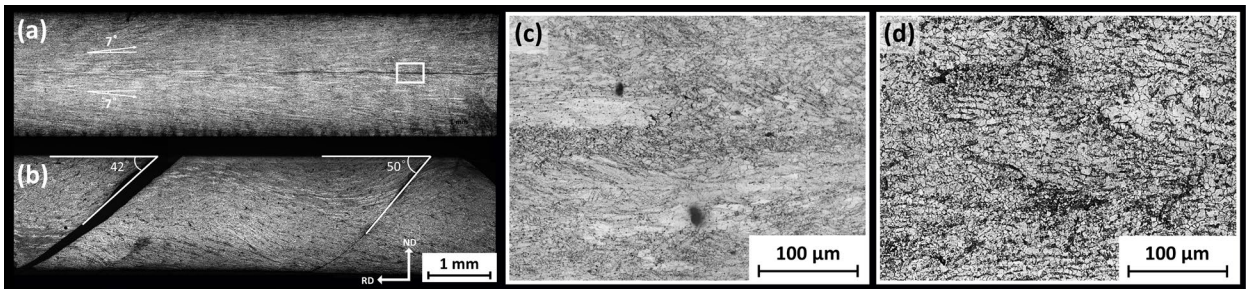

Fig. 3 Optical micrographs of the hot-rolled sheet with the thickness of 2 mm at (a) RD-ND plane (center), (b) RD-ND plane (edge), (c) at the centerline segregation, and (d) RD-TD plane

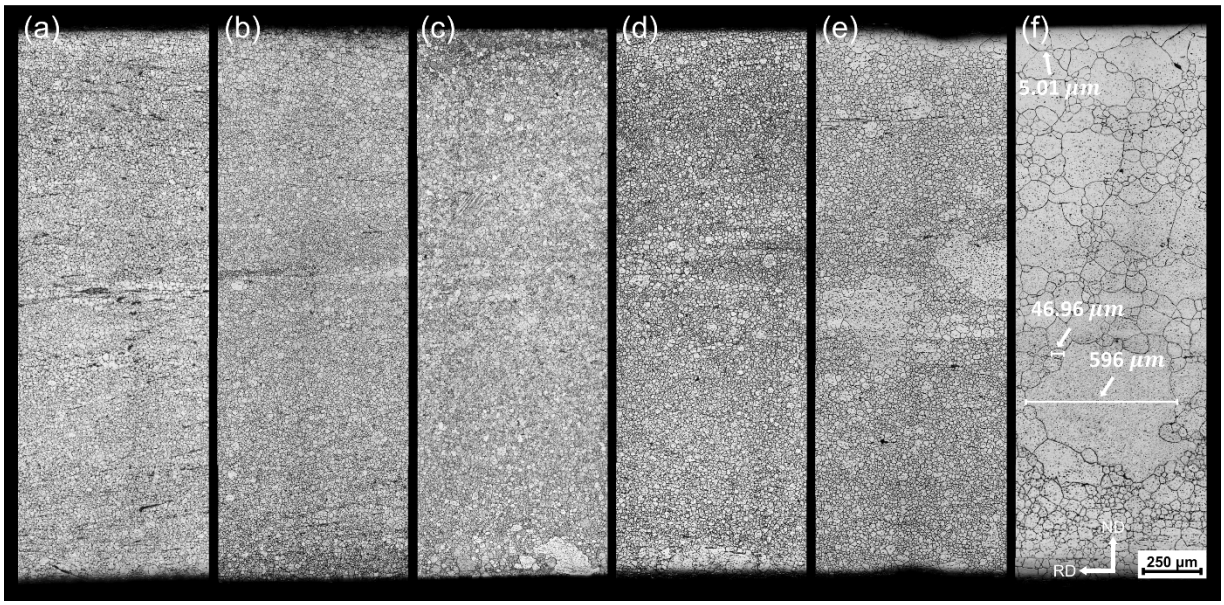

Fig. 4 Optical micrographs of the rolled sheets after the heat treatments at 400℃ for (a) 2 h, (b) 4 h, (c) 8 h, (d) 16 h, (e) 32 h, and (f) 64 h. The optical micrographs at higher magnification are shown in the supplementary materials, Fig. A1.

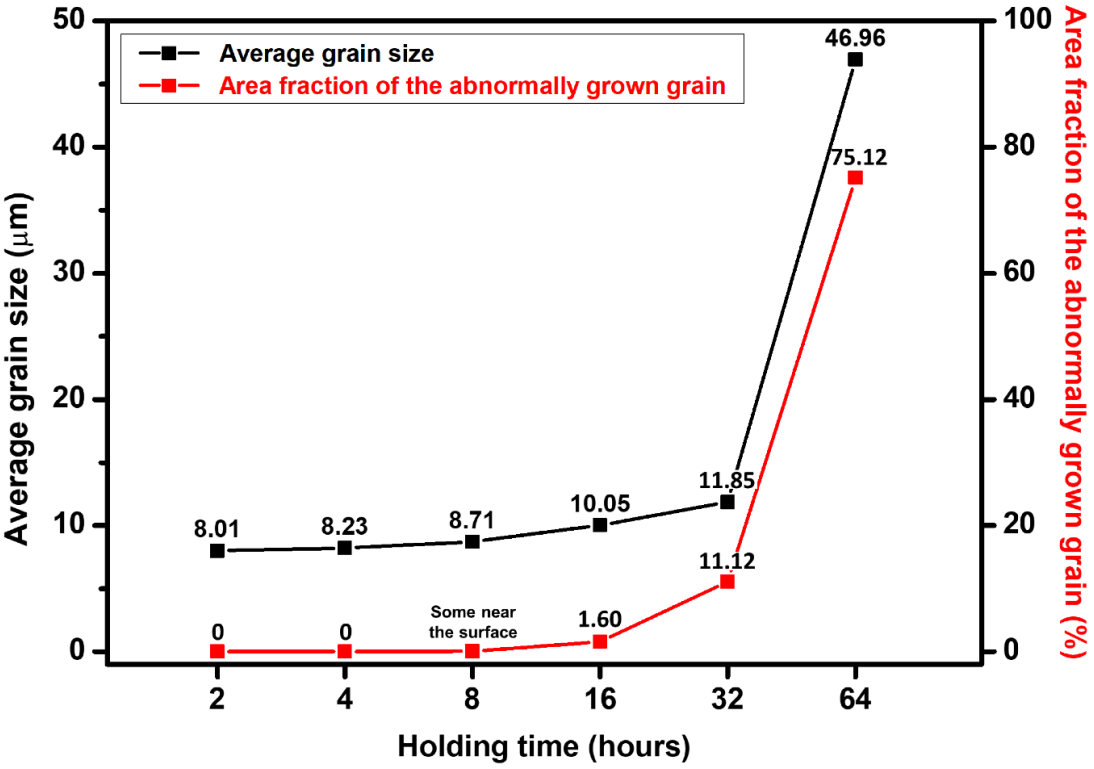

Fig. 5 Average grain size (black) and area fraction of the abnormally grown grains (red), of the rolled sheets after heat treatments at 400℃ for 2, 4, 8, 16, 32, and 64 h

The EDS analysis at different areas of the as-TRC plate and the hot rolled sheet are shown in Table 1, which indicates a severe inhomogeneity of the chemical composition. The intermediate layer between the surface and the mid-thickness area of the as-TRC plate shows columnar grains with dendritic structures, and the chemical composition is similar to the nominal composition. The centerline segregation, as shown in Fig. 2 (b), is related to the high Zn and Ca contents. During the TRC process, the α-Mg matrix (Mg-Zn-Ca solid solution) solidifies from the surface to the mid-thickness area, while Zn and Ca solutes with a relatively small solubility gradually accumulate at the solidification front such that their contents increase in the residual melt. Consequently, the strong segregation of solutes elements is formed at the mid-thickness area that finally solidifies [9, 18, 19]. According to the Mg-0.6Zn-xCa (x = 0 ~ 1wt.%) phase diagram and the solidification simulation by Scheil model calculated by Pandat^{TM} software (Fig. 6), the formation of Mg_2Ca and $Ca_2Mg_5Zn_5$ phases is expected at the dendritic interface [9, 18-22]. The solidification behaviors of Mg-0.6Zn-0.6Ca alloy simulated by using lever rule and Scheil model are presented in the supplementary materials, Fig. A2. Such microstructural inhomogeneity is also observed in the hot-rolled plate. For example, a high content of Zn and Ca at the mid-thickness area and the prior dendritic structures. After the 2 h heat treatment at 400°C, the chemical inhomogeneity of the rolled sheet is diminished, and the fine homogeneous grain structure is observed.

Table 1 Chemical compositions (wt.%) of the examined samples at different states measured by using SEM-EDX

Samples	**Mg**	**Ca**	**Zn**	**Al**	**Zr**
5mm as-TRC plate, area mapping of columnar	Bal.	0.36	0.80	0.29	0.00
5mm as-TRC plate, segregated part of the middle layer	Bal.	1.04	1.93	0.45	0.00
5mm as-TRC plate, point mapping in several points of the columnar edge area	Bal.	3.66	13.43	0.22	0.00
2mm hot-rolled sheet, columnar and fine grain edge area	Bal.	3.92	8.05	0.32	0.16
2mm hot-rolled sheet after homogenization at 400℃ for 2 hours, area mapping	Bal.	0.51	0.59	0.12	0.03

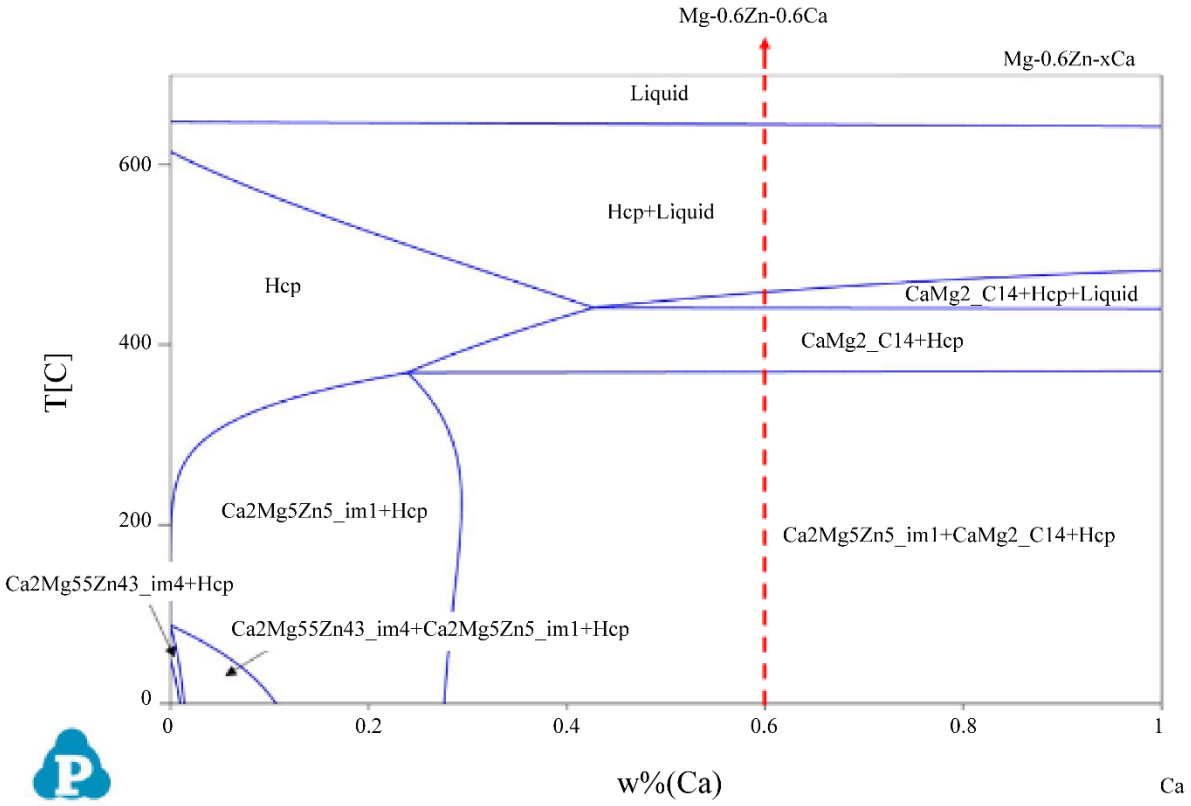

Fig. 6 Phase diagram of Mg-0.6Zn-xCa calculated using thermodynamic simulation software Pandat

The texture of the TRC plate and the rolled sheet and its evolution during the heat treatment is shown in Fig. 7, in terms of the recalculated $(10\bar{1}0)$ and (0002) pole figures. The as-TRC plate has a relatively strong texture with the basal poles slightly spread to the TD, as shown in Fig. 7(a). The strong basal-type texture indicates that the TRC process accompanies a severe rolling deformation of the solidified material. The rolled sheet has a texture type similar to that of the TRC plate. It is generally acknowledged that the symmetric rolling of the Mg alloys results in a basal-type texture [3, 23-25], while the TD spread of the basal poles is generally observed in the Mg alloys containing rare earth elements and/or Ca. The relatively weak texture intensity of the rolled sheet, maximum pole density of the (0002) pole figure, Pmax = 7.92, can be concluded to be a result of the repeated intermediate annealing prior to each rolling step that accompanies the grain refinement and static recrystallization. The texture intensity dramatically decreases with heat treatment of the rolled sheet to Pmax = 3.21 after 2 h. Notably, the heat treatment weakens the basal-poles in the ND and the formation of the basal poles tilted by approximately 20 ° from the ND towards the TD; in other words, altering the basal-type texture to non-basal texture. This characteristic texture is maintained during further heat treatment, while the 32 h heat treated sample shows a high intensity of the (0002) pole figure, Pmax = 6.72. Such high intensity peak is the result of the abnormal grain growth observed in the optical micrographs, as shown in Fig. 4. The intensity peaks

corresponding to the abnormally grown grains are found at various sites of the (0002) pole figure. For example, the single peaks at the lower right part of the (0002) pole figure in Fig. 7(g). Large number of single intensity peaks, that is, abnormally grown grains, are observed in the 64 h heat treated sample. Notably, the single intensity peaks are widely distributed on the pole figures, indicating that the secondary recrystallized grains does not have a preferred orientation.

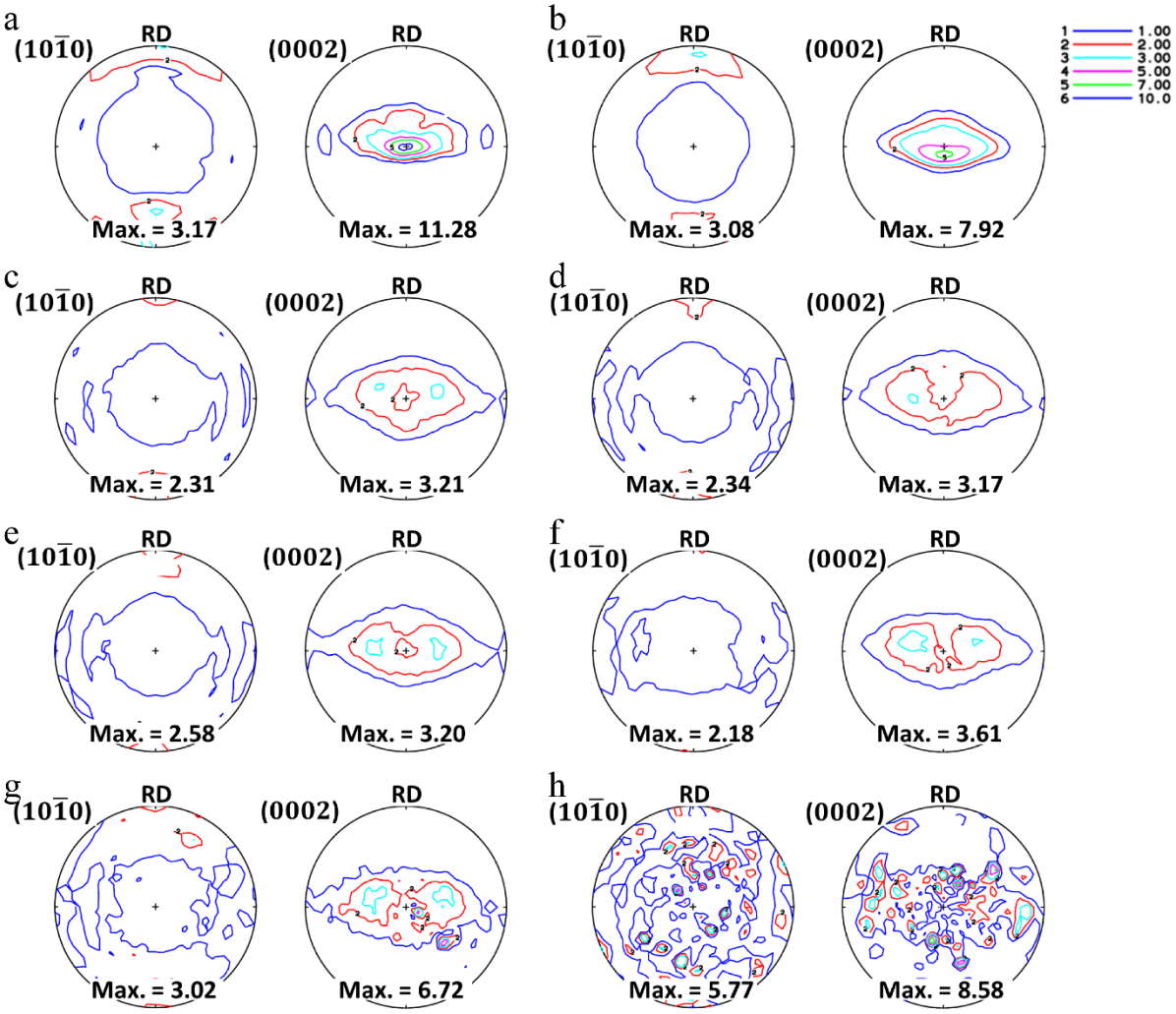

Fig. 7 Recalculated (10$\bar{1}$0) and (0002) pole figures using the 6 measured pole figures from X-ray diffraction (a) as-TRC plate with 5 mm of the thickness, (b) as-rolled sheet with 2 mm of the thickness, and after the heat treatments at 400 °C for (c) 2 h, (d) 4 h, (e) 8 h, (f) 16 h, (g) 32 h, and (h) 64 h

To examine the relationship between the grain growth and the texture development during the heat treatment, EBSD measurements were conducted on the heat-treated sheets. To ensure grains statistics, EBSD scans were conducted on a large area of 1900 × 1500 μm^2, such that the EBSD texture is similar to that from the XRD measurements. Fig. 8 illustrates the EBSD inverse pole figure (IPF) maps and the texture of the 16 h heat

treated sample. For comparison of textures between the grains with different sizes, the 16 h heat treated sample is selected because it has various groups of grains, from some to tens of μm. The texture of the whole EBSD area, as shown in Fig. 8 (a), can be described as the basal pole tilted approximately 20° ~ 30° to the TD and the $10\bar{1}0$ poles in the RD, which is a characteristic texture of the rolled sheet of RE and/or Ca containing Mg alloys sheets after recrystallization annealing. The small grains with the size of 0 ~ 5 μm, as shown in Fig. 8 (b), have an area fraction of 1.0 % and they show a similar texture in the whole area. Additionally, similar feature in texture is found in the grains with 5 ~ 10 μm, as shown in Fig. 8 (c). These two groups of small grains show the basal poles tilted in the TD and RD, which were reported as a quarto-distribution or round-shape distribution of the basal pole [26, 27]. The grains with the size of 10 ~ 20 μm are dominant with the area fraction of 60.8%, as shown in Fig. 8 (d); they reflect the texture of the whole area. The grains with the size of 20 ~ 30 μm, which are approximately two times larger than the average grain size, as shown in Fig. 8 (e), have a larger scatter of the orientations, while they still maintain the feature of the basal poles tilted in the TD. The grains larger than 30 μm have an area fraction of 4.7% and they show the more randomly distributed orientations, as shown in Fig. 8 (f), compared to the groups of the smaller grains. These results show that the secondary recrystallization of the present 0.6Zn-0.6Ca-Mg sheet does not relate to the preferred growth of specific orientations. Additionally, the orientation relationship of a growing grain with its neighboring grains was analyzed through misorientation across the grain boundaries. The IPF map of the 32 h heat treated sample is illustrated in Fig. 9 (a), and the growing grains selected for the misorientation analysis are shown in Fig. 9 (b) and (c). The boundaries selected for the misorientation analysis are marked with arrows on the figures, and the corresponding misorientation relations between the beginning and the ends of the arrows are given in Table 2. The analyzed boundaries mostly have a concave shape, indicating that they will consume the neighboring small grains as they move during further heat treatments. Similar to the orientation of the growing grains, there is no clear preference in the misorientation axis and misorientation angle of the boundaries of the growing grains. That is, the secondary recrystallization is not driven by the grain boundary characteristics, like boundary energy. The kernel average misorienation (KAM) map of the 32 h heat treated sample is shown in the Fig. 9 (d). KAM is the local misorientation around each EBSD measuring point, and it is often used as a measure showing the stored energy in a deformed material. The growing grains, marked with white dashed circles, with a low KAM value are mostly surrounded by the small grains with relatively large KAM values. Notably there are some large growing grains that have the opposite tendency, which is, marked with orange circles. Based on the above results, it is

reasonable to conclude that the secondary recrystallization observed in the present study is mainly driven by the reduction of the stored energy and the size benefit of the large grains.

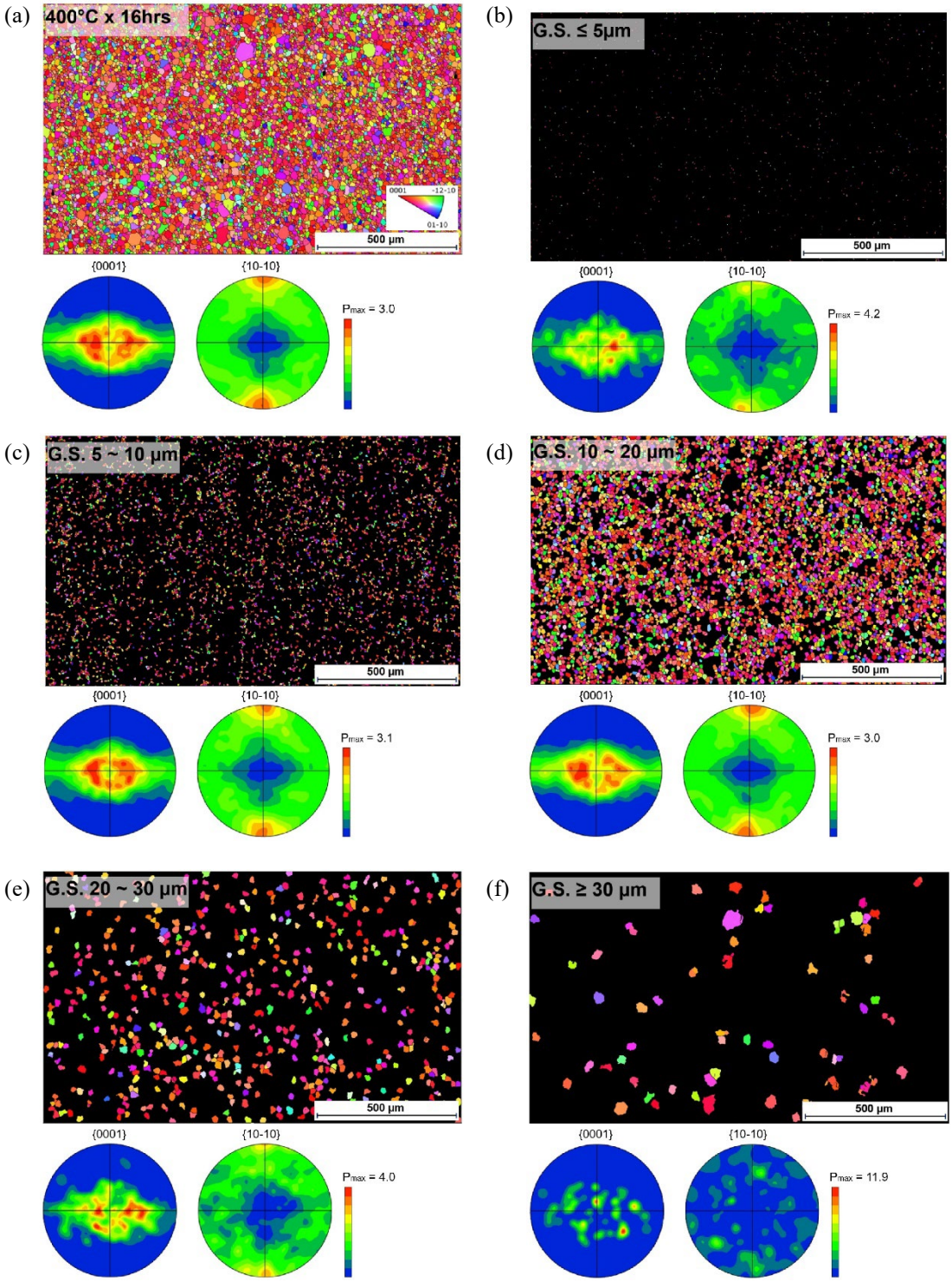

Fig. 8 (a) EBSD IPF map in the ND and pole figures of the heat-treated sample at 400°C for 16 h, and the same evaluated from the grains classified by the ranges of the grain sizes, (b) smaller than 5 μm, (c) 5 ~ 10 μm, (d) 10 ~ 20 μm, (e) 20 ~ 30 μm and (f) larger than 30 μm. The grain sizes were estimated by the equivalent circular diameters from the EBSD measurement

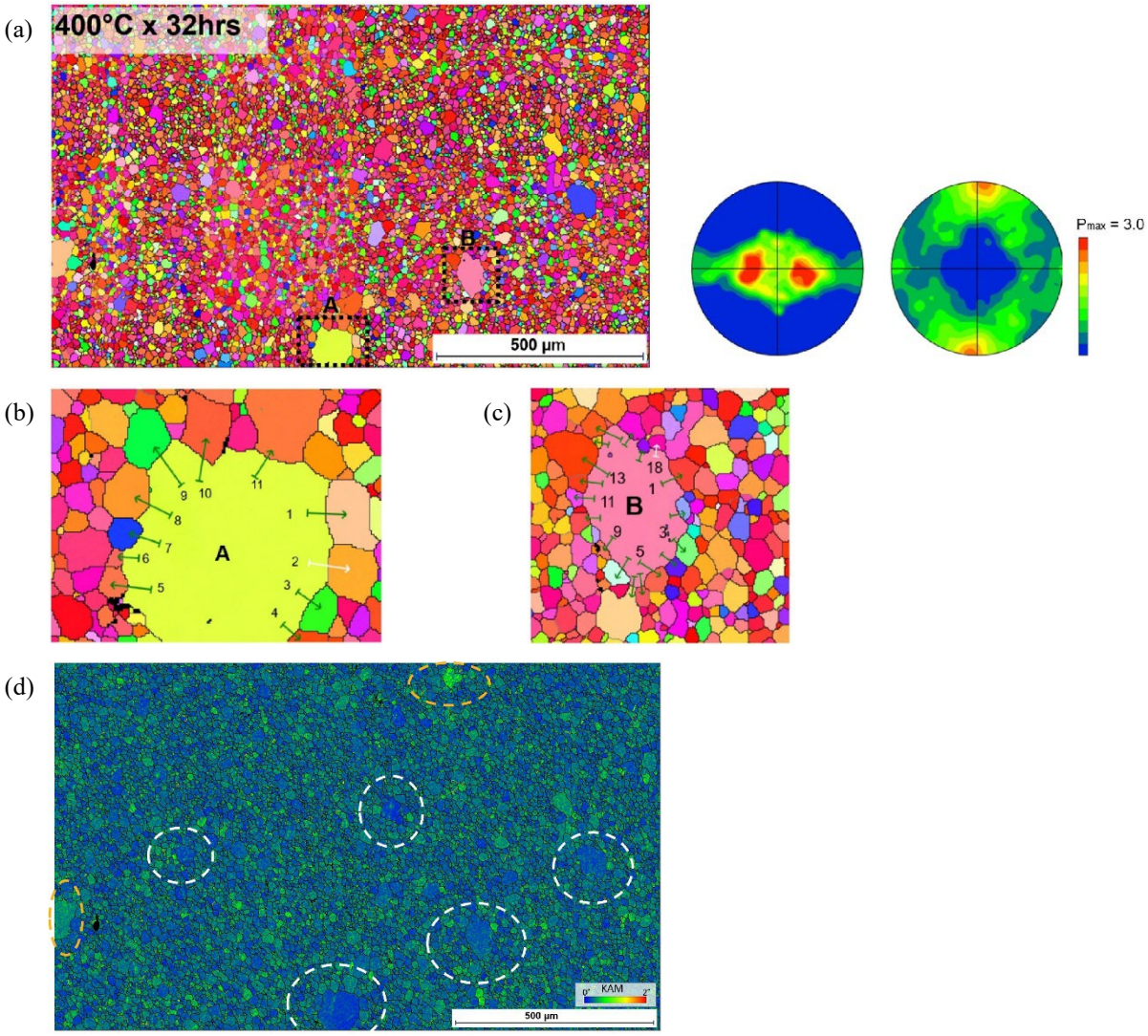

Fig. 9 (a) EBSD IPF map in the ND and pole figures of the heat-treated sample at 400°C for 32 h (b) and (c) abnormally grown grains selected for the misorientation analysis with the neighboring grains. (d) Kernel average misorientation (KAM) map, within the angular range from 0° (blue) to 2° (red). The black squares marked on Fig. 9 (a) indicate the coarse grains for the misorientation analysis. The misorientation relationships with the neighboring grains, marked with the arrows in Fig. 9 (b) and (c), are shown in Table 2.

Table 2 Misorientation relationships of the abnormally grown grains with the neighboring grains in the 32 h heat-treated sample. Grains A and B correspond to the Fig. 9 (b) and (c), respectively

	Grain A		Grain B	
Nr.	Misorientation angle	Misorientation axis	Misorientation angle	Misorientation axis
1	32.5°	<1 $\bar{2}$ 1 $\bar{4}$>	28.5°	<3 $\bar{3}$ 0 $\bar{1}$>
2	90.5°	<10 $\bar{11}$ 1 $\bar{3}$>	79.3°	<7 $\bar{8}$ 1 $\bar{3}$>
3	80.5°	<10 $\bar{11}$ 1 $\bar{3}$>	55.6°	<8 $\bar{7}$ $\bar{1}$ 0>
4	51.1°	<$\bar{1}$ $\bar{4}$ 5 $\bar{3}$>	76.2°	<8 $\bar{10}$ 2 $\bar{3}$>
5	74.7°	<3 $\bar{2}$ $\bar{1}$ $\bar{1}$>	51.3°	<$\bar{7}$ 2 5 $\bar{3}$>
6	86.9°	<$\bar{3}$ 3 0 $\bar{1}$>	56.5°	<2 $\bar{3}$ 1 $\bar{1}$>
7	76.6°	<11 $\bar{10}$ $\bar{1}$ $\bar{6}$>	79.1°	<11 $\bar{10}$ $\bar{1}$ 0>
8	20.1°	<$\bar{10}$ 11 $\bar{1}$ $\bar{6}$>	57.6°	<$\bar{1}$ $\bar{1}$ 2 $\bar{1}$>
9	91.5°	<$\bar{8}$ 10 $\bar{2}$ $\bar{3}$>	53.9°	<$\bar{7}$ 2 5 $\bar{3}$>
10	38.8°	<$\bar{2}$ $\bar{5}$ 7 $\bar{3}$>	81.0°	<2 $\bar{2}$ 0 $\bar{1}$>
11	64.9°	<10 $\bar{11}$ 1 $\bar{3}$>	31.0°	<$\bar{1}$ $\bar{1}$ 2 $\bar{3}$>
12			43.0°	<-1 $\bar{4}$ 5 0>
13			39.4°	<10 $\bar{11}$ 1 0>
14			33.4°	<1 $\bar{5}$ 4 $\bar{9}$>
15			43.2°	<$\bar{2}$ 0 2 $\bar{1}$>
16			64.2°	<-1 $\bar{1}$ 2 0>
17			63.4°	<$\bar{2}$ 1 1 0>
18			82.6°	<7 $\bar{8}$ 1 $\bar{3}$>

Additionally, the formation and dissolution of the secondary phases during the thermomechanical treatments should be considered to address their influence on the secondary recrystallization. According to the

thermodynamic calculation, as shown in Fig. 6, the secondary phases existing in the rolled sheet are the Mg_2Ca and $Ca_2Mg_5Zn_5$ phases. The static recrystallization commences at the deformed microstructure by conducting the heat treatment of the rolled sheet at 400°C. The Mg_2Ca and $Ca_2Mg_5Zn_5$ phases can act as nucleation site of the recrystallization in case that the size of the precipitates is large enough, which is usually larger than 1 μm, for triggering the particle stimulated nucleation (PSN) [28]. However, the precipitates observed in the rolled sheet are mostly fine, and it is deduced that the PSN restrictively contributes to the recrystallization and the formation of the weak texture. The role of the precipitates on the recrystallization can be considered as a pinning mechanism of the grain boundary motion. As a result, the average grain sizes are maintained at a similar level for 16 h of heat treatment, as shown in Fig. 5. The secondary phases, $Ca_2Mg_5Zn_5$ and a part of Mg_2Ca, are dissolved as the heat treatment is prolonged to 32 h at 400°C, and the grain boundaries can easily move while encroaching the surrounding fine grains. It is to point out that the heat treatment at 340°C, which corresponds to the area of (Mg) matrix, $Ca_2Mg_5Zn_5$ and Mg_2Ca in the equilibrium phase diagram, does not bring out the rapid grain growth such that the average grain size of 17.7 μm is remained in the annealed sample for 512 h [29]. This elucidates the appearance of the abnormal grain growth at the near surface area of the 16 h heat treated sheet. Due to the nature of the TRC process, the density of the secondary phases is smaller at the near surface area, where the solidification occurs firstly during the TRC process. Therefore, the dissolution of the secondary phases occurs earlier near the surface area, such that the pinning effect of the grain boundary motion is diminished. The more precipitates are dissolved by increasing the heat treatment time, the more grains can grow abnormally. Additionally, these results indicate that the selection of alloying elements and the thermal stability of the secondary phases play an important role in controlling the recrystallization behavior and abnormal grain growth.

4. Conclusion

In the present work, the microstructural evolution of 0.6Zn-0.6Ca-Mg alloy plate manufactured by the TRC process was investigated during hot rolling and heat treatment at 400 °C by focusing on the occurrence of secondary recrystallization. The possible mechanisms of the abnormal grain growth was evaluated by optical microscopy, texture analysis, and EBSD. Therefore, the following conclusions can be drawn:

1. The microstructural inhomogeneity of the as-TRC plate with 5 mm thickness is described by the centerline segregation and the columnar structure inclined in the RD. The centerline segregation is partly

observed even after the hot rolling to 2 mm of thickness, and the mixture of the remaining dendritic cast structure and partially recrystallized grains.

2. The inhomogeneous microstructure of the rolled sheet, such as the remaining cast structure, vanished and fully recrystallized structure with globular grains appeared after the heat treatment at 400°C for 2 h. With the increased heat treatment time, some abnormally grown grains were observed, which first developed at the surface near area, e.g. after 16 h heat treatment, and evolved towards the mid-volume of the sheet as the heat treatment time was increased.
3. The abnormally grown grains have no preference in the orientation and the misorientation relationship to the neighboring grains. The EBSD analysis confirmed that the abnormal grain growth is mainly driven by the reduction of stored energy and the size benefit of larger grains. Moreover, the secondary recrystallization is triggered by the dissolution of fine secondary phases, which suppress the boundary motion after long-term annealing.
4. A strong basal-type texture was developed In the rolled sheet, in which the basal poles were slightly spread in the TD. The heat treatment induced a significant texture weakening and the formation of non-basal texture with the basal poles tilted 30° in the TD. By occurrence of the secondary recrystallization the strong single peaks were observed, where their orientations were randomly distributed.

Statements and Declarations

Funding: This research was supported by Kumoh National Institute of Technology (2021). Financial support of BrainPool Program (Grant nr. 2021H1D3A2A0208305) of National Research Foundation and KIMS Academy Lab program (PNK8660) for the research stay of SYi at KIMS is gratefully acknowledged.

Competing interests: The authors declare no competing financial interests or personal relationships that could have appeared to influence the work reported in the present paper.

Availability of data and materials: The datasets used and/or analyzed during the current study are available from the corresponding author on reasonable request.

Code availability: Not applicable.

Authors' contributions: Conceptualization: [N.-J. Park, S. Yi, D. Letizg]; Methodology: [H.J. Lee, S. Yi]; Formal analysis and investigation: [H.J. Lee, S.Yi]; Writing - original draft preparation: [H.J. Lee, S. Yi]; Writing - review and editing: [H.J. Lee, S. Yi, N.-J. Park, D. Letzig]; Funding acquisition: [N.-J. Park]; Resources: [H.J. Lee, S. Yi, D. Letzig]; Supervision: [N.-J. Park, S. Yi].

Ethics approval: Not applicable.

Consent to participate: Not applicable.

Consent for publication: Not applicable.

References

1. J. D. Sim, Korea Institute of Science and Technology Information, ReSEAT Research Report (2016)
2. W.J. Joost, P.E. Krajewski, Scripta Mater. 128, 107 (2017)
3. D. Klaumuenzer, J. Victoria-Hernandez, S. Yi, D. Letzig, S. H. Kim, J. J. Kim, M. H. Seo, K. Ahn, Magnesium Technology 2019 (eds) V. Joshi., J. Jordon, D. Orlov, N. Neelameggham, 15 (2019)
4. Y. B. Chun, Metall. Mater. Trans. A, 42, 4113 (2011)
5. Y. N. Wang, J. C. Huang, Mater. Chem. Phys., 81, 11 (2003)
6. S. H. Kim, B. S. You, C. D. Yim, Y. M. Seo, Mater. Lett., 59, 3876 (2005)
7. J. J. Kim, W. J Park, D, Choo, Magnesium Technology 2011 (eds) Wim H. Sillekens, Sean R. Agnew, Neale R. Neelameggham, Suveen N. Mathaudhu, 147 (2011)
8. M. A. Wells, A. Hadadzadeh, Mater. Sci. Forum, 783-786, 527 (2014)
9. H. J. Lee, N. J. Park, J. Korean Soc. Heat Treat., 34, 122 (2021)
10. L. Shi, H. Lv, M. Li, T. Zhou, M. Yang, Met. Mater. Int., 28, 1224 (2022)
11. J.W. Park, S.J. Park, K.S. Shin, Met. Mater. Int., 23, 444 (2017)
12. J. Go, J.U. Lee, B.G. Moon, J. Yoon, S.H. Park, Met. Mater. Int, 26, 1779 (2020)
13. H. Bessemer, Improvement in manufacture of iron and steel, US Patent 49053 (1865)
14. M. Yun, S. Lokyer, J. D. Hunt, Mater. Sci. Eng. A, 280, 116 (2000)
15. R. Cook, P. G. Grocock, P. M. Thomas, D.V. Edmonds, J.D. Hunt, J. Mater. Proc. Technol., 55, 76 (1995)
16. S.J. Park, H.C. Jung, K.S. Shin, Met. Mater. Int., 22, 1055 (2016)
17. H. J. Bunge, Texture Analysis in Materials Science, Butterworths, 47 (1982)
18. H. R. Bakhsheshi-Rad, M. R. Abdul-Kadir, M. H. Idris, S. Farahany, Corros. Sci., 64, 184 (2012)
19. J. Victoria-Hernández, G. Kurz, J. Bohlen, S.B. Yi, D. Letzig, JOM, 73, 1460 (2021)
20. R. Hou, J. Victoria-Hernandez, P. Jiang, R. Willumeit-Römer, B. Luthringer-Feyerabend, S. Yi, D. Letzig, F. Feyerabend, Acta Biomaterialia, 97, 608 (2019)
21. K. Oh-ishi, R. Watanabe, C. L. Mendis, K. Hono, Mater. Sci. Eng. A, 526, 177 (2009)
22. S. E. Harandia, M. Mirshahia, S. Koleinia, M. H. Idrisa, H. Jafari, M. R. A. Kadir, Mater. Res., 16, 11 (2013)
23. C. W. Ha and N. J. Park, Korean J. Met. Mater., 52, 589 (2014)
24. G.T. Bae, J.H. Bae, D.H. Kang, H. Lee, Nack J. Kim, Met. Mater. Int., 15, 1 (2009)

25. B. Shin, H. Kang, D. Bae, Met. Mater. Int., 18, 23 (2012)

26. S. Yi, J. Victoria-Hernandez, Y. M. Kim, D. Letzig, B. S. You, Metals 9, 181 (2019)

27. D. Steglich, Y. Jeong, Korean J. Met. Mater., 117, 102 (2016)

28. J. D. Robson, D. T. Henry, B. Davis, Acta Materialia, 57, 2739 (2009)

29. H.J. Lee, N.J. Park, J. Korean Soc. Heat Treat., 35, 74 (2022)